10.24425/acs.2019.130202

Archives of Control Sciences
Volume 29(LXV), 2019
No. 3, *pages 485–506*

A new 4-D dynamical system exhibiting chaos with a line of rest points, its synchronization and circuit model

SUNDARAPANDIAN VAIDYANATHAN, ACENG SAMBAS and SEN ZHANG

A new 4-D dynamical system exhibiting chaos is introduced in this work. The proposed nonlinear plant with chaos has an unstable rest point and a line of rest points. Thus, the new nonlinear plant exhibits hidden attractors. A detailed dynamic analysis of the new nonlinear plant using bifurcation diagrams is described. Synchronization result of the new nonlinear plant with itself is achieved using Integral Sliding Mode Control (ISMC). Finally, a circuit model using MultiSim of the new 4-D nonlinear plant with chaos is carried out for practical use.

Key words: chaos, chaotic systems, circuit design, synchronization

1. Introduction

In science and engineering, much research attention has been devoted to the modelling and applications of dynamical systems having chaotic behaviour [1, 2]. Chaotic systems are useful in applications such as mechanical systems [3–7], secure communication [8, 9], neurology [10–12], steganography [13, 14], cryptosystems [15,16], chemical reactors [17–19], ecology [20], finance [21], etc.

Chaos theory has significant applications in transmission and communication engineering. Recently, Liu [22] suggested a direct acquisition algorithm using chaotic sequences to improve the communication systems based on chaotic DSSS signals, which aids in overcoming difficulties in different acquisition problems.

S. Vaidyanathan (corresponding author) is with School of Electrical and Computing, Vel Tech University, 400 Feet Outer Ring Road, Avadi, Chennai-600092, Tamil Nadu, India. E-mail: sundarvtu@gmail.com

Department of Mechanical Engineering, Universitas Muhammadiyah Tasikmalaya, Tasikmalaya 46196, West Java, Indonesia, E-mail: acengs@umtas.ac.id

School of Physics and Opotoelectric Engineering, Xiangtan University, Xiangtan 411105, Hunan, China. E-mail: SenS_Zhang@163.com

Received 27.02.2019.

For secure systems, Wang and Li [23] devised a color image encryption method which is constructed using Hopfield chaotic neural network. Hua et al. [24] treated the image encryption problem by proposing a cosine-transform-based chaotic system, which is useful in cryptography. Gohari et al. [25] suggested an algorithm for 3-D planning using chaotic maps for the motion planning and regulation of a quadrotor for boundary surveillance applications. Naseer et al. [26] gave a new approach to improve the security of multimedia systems using a chaotic map. Karakaya et al. [27] built a memristive chaotic circuit and discussed also FPGA implementation and TRBG based on it. Wang and Dong [28] dealt with a 4-D autonomous quadratic hyperchaotic system from the classical Lorenz system and built an electronic circuit design.

This work describes a new 4-D dynamical system with only two quadratic nonlinearities. It is shown that the proposed chaotic system the new nonlinear plant has an unstable rest point and a line of rest points. Thus, the new nonlinear plant exhibits hidden attractors [1, 2].

As a control application, we discuss global chaos synchronization of the new nonlinear plant with itself using Integral Sliding Mode Control (ISMC). Sliding mode control has many advantages in control theory such as order reduction, decoupling design procedures, disturbance rejection and insensitivity to small parameter variations [29, 30].

Finally, a circuit model using MultiSim of the new nonlinear plant with chaos is carried out for practical use.

2. A new chaotic dynamical system with a line of rest points

In this work, we propose a nonlinear plant given by

$$\begin{cases} \dot{x} = a(y-x)+w, \\ \dot{y} = x(b-z), \\ \dot{z} = xy-cz, \\ \dot{w} = r-ay-w, \end{cases} \tag{1}$$

where $X=[x, y, z, w]^T$ is the state vector and a, b, c, r are constant parameters.

In this work, we shall show that the plant (1) exhibits *chaos* for the choice of parameter values

$$a=10, \quad b=20, \quad c=3, \quad -1 \leqslant r \leqslant 1. \tag{2}$$

Throughout this section, we fix the values of a, b and c as $(a, b, c)=(10, 20, 3)$. We consider r in the range $-1 \leqslant r \leqslant 1$.

To determine the rest points of the plant (1), we solve the system

$$a(y - x) + w = 0, \tag{3a}$$
$$x(b - z) = 0, \tag{3b}$$
$$xy - cz = 0, \tag{3c}$$
$$r - ay - w = 0. \tag{3d}$$

From Eq. (3d), we have

$$r = ay + w. \tag{4}$$

Thus, we can eliminate w from (3) and rewrite it as

$$r - ax = 0, \tag{5a}$$
$$x(b - z) = 0, \tag{5b}$$
$$xy - cz = 0. \tag{5c}$$

When $r = 0$, the system (5) can be solved as

$$x = 0, \qquad z = 0, \qquad ay + w = 0 \tag{6}$$

which is a line of rest points in the (y, w)-plane.

When $r \neq 0$, the system (5) can be solved as

$$x = \frac{r}{a}, \qquad z = b, \qquad y = \frac{cz}{x}. \tag{7}$$

Since $w = r - ay$, we have a single rest point given by

$$x = \frac{r}{a}, \qquad y = \frac{abc}{r}, \qquad z = b, \qquad w = \frac{r^2 - a^2bc}{r}. \tag{8}$$

Thus, the nonlinear plant (1) has a line of rest points (6) when $r = 0$ and the single rest point (8) when $r \neq 0$.

Lyapunov exponents of the nonlinear plant (1) are calculated for $(a, b, c, r) = (10, 20, 3, 0)$ and $X(0) = [0.2, 0.2, 0.2, 0.2]^T$ for $T = 1E4$ seconds as

$$LE_1 = 0.5182, \qquad LE_2 = 0, \qquad LE_3 = -0.1703, \qquad LE_4 = -14.3479. \tag{9}$$

From Eq. (9), it is clear that the nonlinear plant (1) is chaotic and dissipative when $r = 0$.

Lyapunov exponents of the nonlinear plant (1) are calculated for $(a, b, c, r) = (10, 20, 3, 1)$ and $X(0) = [0.2, 0.2, 0.2, 0.2]^T$ for $T = 1E4$ seconds as

$$LE_1 = 0.5206, \qquad LE_2 = 0, \qquad LE_3 = -0.1704, \qquad LE_4 = -14.3502. \quad (10)$$

From Eq. (10), it is clear that the nonlinear plant (1) is chaotic and dissipative when $r = 1$.

Similarly, the Lyapunov exponents of the nonlinear plant (1) are calculated for $(a, b, c, r) = (10, 20, 3, -1)$ and $X(0) = [0.2, 0.2, 0.2, 0.2]^T$ for $T = 1E4$ seconds as

$$LE_1 = 0.5227, \qquad LE_2 = 0, \qquad LE_3 = -0.1704, \qquad LE_4 = -14.3523. \quad (11)$$

From Eq. (11), it is clear that the nonlinear plant (1) is chaotic and dissipative when $r = -1$.

By calculating the Lyapunov exponents of the nonlinear plant (1), it is also easy to show that the plant (1) is chaotic and dissipative for all values of r in $0 < r < 1$ and $-1 < r < 0$.

We also note that the nonlinear plant (1) stays invariant under the change of state coordinates displayed by

$$(x, y, z, w) \mapsto (-x, -y, z, -w). \quad (12)$$

This pinpoints rotation symmetry of the nonlinear plant (1) about $z = 0$ and highlights an important property that every non-zero trajectory of the plant (1) has a twin trajectory.

For the chaotic case $(a, b, c, r) = (10, 20, 3, 1)$, the nonlinear plant (1) has a unique rest point given by $X_0 = [0.1, 600, 20, -5999]^T$. We calculate that

$$J(X_0) = \begin{bmatrix} -10 & 10 & 0 & 1 \\ 0 & 0 & -0.1 & 0 \\ 600 & 0.1 & -3 & 0 \\ 0 & -10 & 0 & -1 \end{bmatrix}. \quad (13)$$

The linearization matrix $J(X_0)$ has the spectral values

$$\phi_1 = -0.0002, \qquad \phi_2 = -14.1154, \qquad \phi_{3,4} = 0.0578 \pm 6.6810i. \quad (14)$$

Thus, the rest point X_0 is a saddle-focus, which is unstable.

Similarly, for the chaotic case $(a, b, c, r) = (10, 20, 3, -1)$, the nonlinear plant (1) has a unique rest point given by $Y_0 = [-0.1, -600, 20, 5999]^T$. It is easy to check that the matrix $J(Y_0)$ has the same spectral values as $J(X_0)$. Hence, the rest point Y_0 is a saddle-focus, which is unstable.

The phase plots of the nonlinear plant (1) are shown in Figs 1–4 with the values $(a, b, c, r) = (10, 20, 3, 0)$ for the parameters and $X(0) = [0.2, 0.2, 0.2, 0.2]^T$ for the initial state of the nonlinear plant (1).

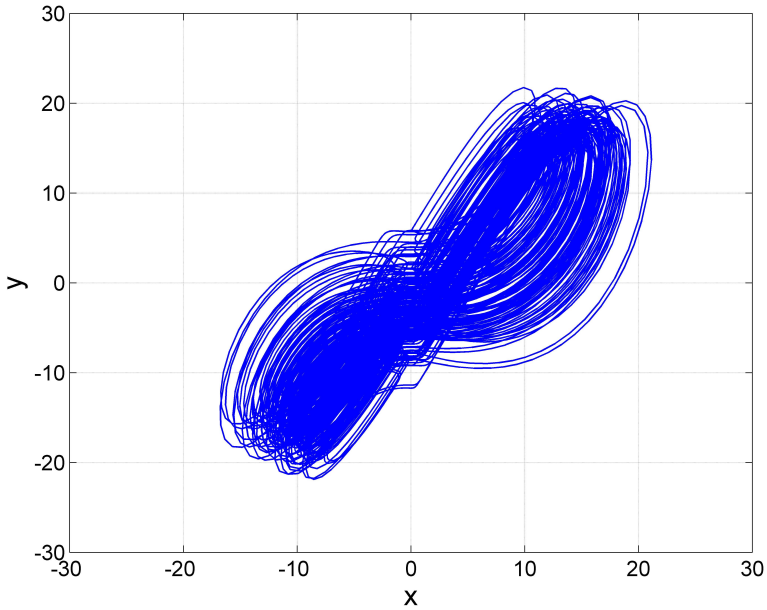

Figure 1: The phase signal plot of the nonlinear plant (1) simulation in MATLAB in the (x, y)-plane with $(a, b, c, r) = (10, 20, 3, 0)$ and $X(0) = [0.2, 0.2, 0.2, 0.2]^T$.

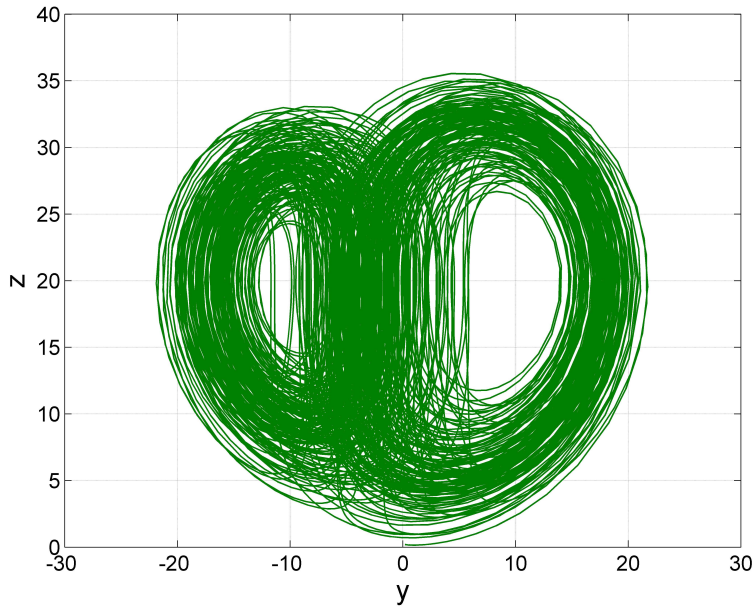

Figure 2: The phase signal plot of the nonlinear plant (1) simulation in MATLAB in the (y, z)-plane with $(a, b, c, r) = (10, 20, 3, 0)$ and $X(0) = [0.2, 0.2, 0.2, 0.2]^T$.

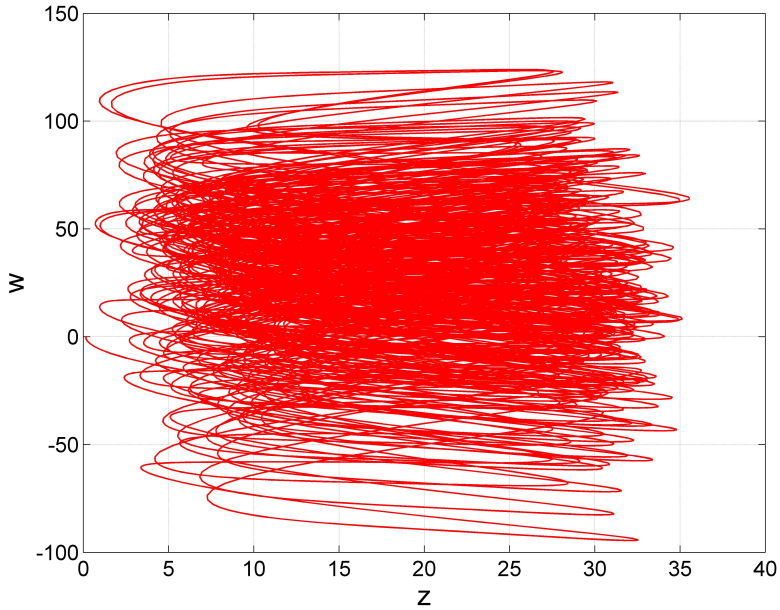

Figure 3: The phase signal plot of the nonlinear plant (1) simulation in MATLAB in the (z, w)-plane with $(a, b, c, r) = (10, 20, 3, 0)$ and $X(0) = [0.2, 0.2, 0.2, 0.2]^T$.

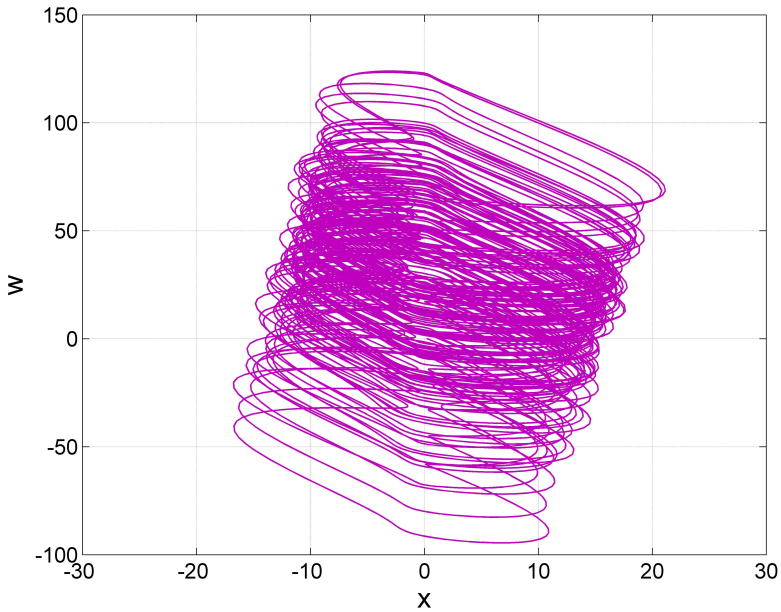

Figure 4: The phase signal plot of the nonlinear plant (1) simulation in MATLAB in the (x, w)-plane with $(a, b, c, r) = (10, 20, 3, 0)$ and $X(0) = [0.2, 0.2, 0.2, 0.2]^T$.

3. Bifurcation analysis of the new 4-D chaotic system

The bifurcation diagram, as a significant tool, is commonly applied for conducting a qualitative study of the dynamics of a nonlinear system [31, 32]. To present the dynamics of the system (1), we plot the bifurcation diagram of the state y and the corresponding Lyapunov characteristic exponents of the system (1) as shown in Fig. 5 with the parameter r taking values in $[-1, 1]$, fixing other parameters as $a = 10$, $b = 20$, $c = 3$ and the initial state as $(0.2, 0.2, 0.2, 0.2)$. As can be seen from Fig. 5b, all the Lyapunov exponents are unchanged and the largest Lyapunov exponent of the system (1) is positive, which means that the system (1) is in robust chaotic state and has a unique property of constant Lyapunov exponents [31, 32].

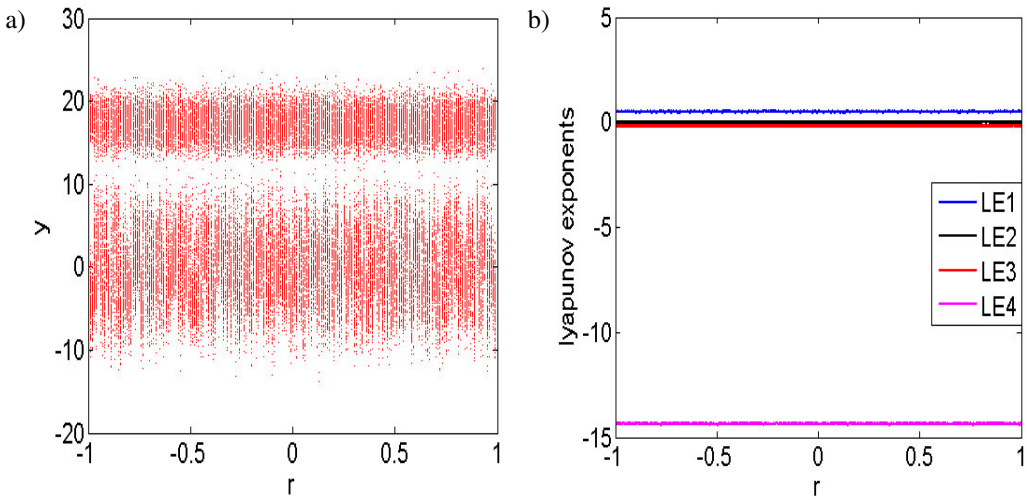

Figure 5: Dynamics of the system (1): a) bifurcation diagram of the state variable y with respect to the control parameter r, b) the corresponding Lyapunov exponents spectrum.

Additionally, multi-stability means the coexistence of two or more attractors with the same parameter set but with different initial values. Multi-stability can lead to very complex behaviors and it has been found in many dynamical systems [33, 34]. Fix $a = 10$, $b = 20$, $r = 1$, and keep c as the control parameter in the dynamic analysis of the system (1). When c is varied in $[2, 3]$, the coexisting bifurcation model of the state y and the corresponding Lyapunov exponents (for better clarity, only the three largest Lyapunov exponents are presented, and the missing ones have smaller negative values) are plotted in Figs 6a and 6b, respectively, where the blue orbit starts from the initial state $(0.2, 0.2, 0.2, 0.2)$ and the red orbit starts from the initial state $(-0.2, -0.2, 0.2, -0.2)$. From Fig. 6a, we can observe some kinds of coexisting attractors with different initial conditions.

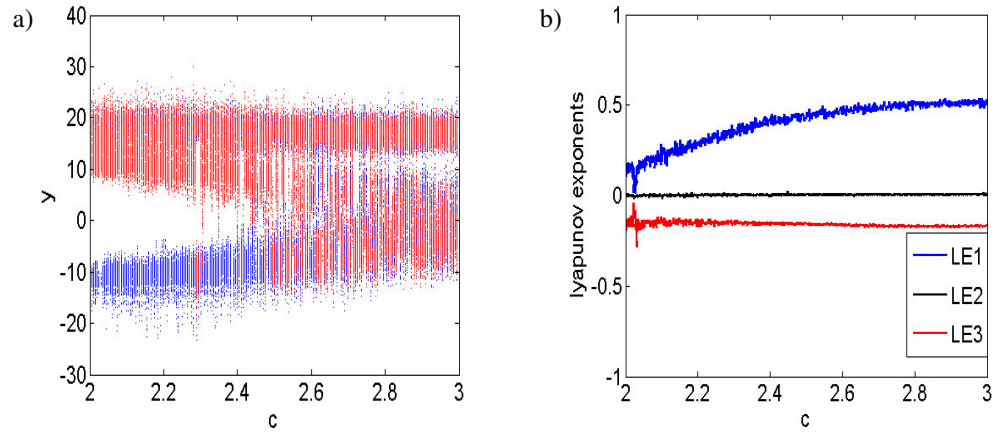

Figure 6: Dynamics of the system (1): a) coexisting bifurcation diagram of the state y with respect to the control parameter c, b) the first three corresponding Lyapunov exponents spectrum with the initial state $(0.2, 0.2, 0.2, 0.2)$. Note that the blue trajectory begins with the initial state $(0.2, 0.2, 0.2, 0.2)$ and the red trajectory begins with the initial state $(-0.2, -0.2, 0.2, -0.2)$.

Figure 7 exhibits the coexisting chaotic attractors with $c = 2.2$ and the coexisting periodic and chaotic attractors with $c = 2.022$, where the blue attractor begins with the initial state $(0.2, 0.2, 0.2, 0.2)$ and the red one begins with $(-0.2, -0.2, 0.2, -0.2)$. Particularly, from Fig. 6b it can be seen that the system starts from a chaotic orbit in the beginning and then evolves into an extremely narrow period window and then goes into chaos again with the control parameter c increasing in the region of $[2, 3]$.

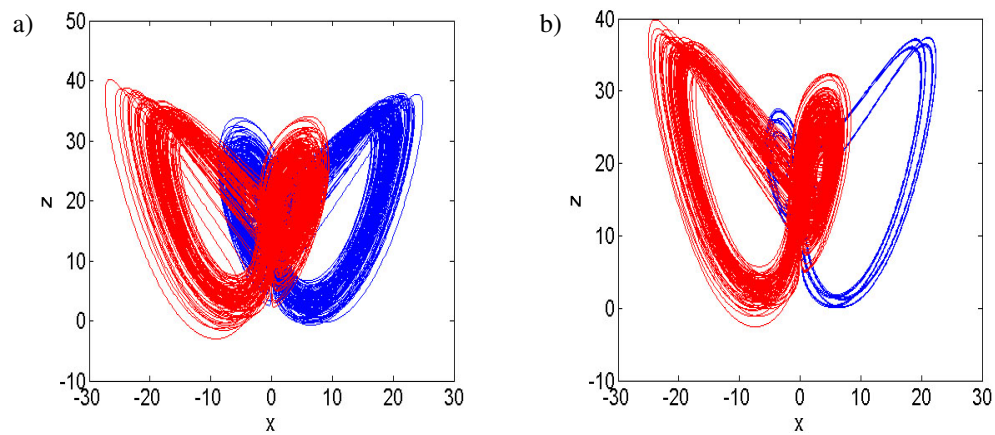

Figure 7: Different coexisting attractors of the system (1): a) coexisting chaotic attractors with $c = 2.2$, b) coexisting period attractor and chaotic attractor with $c = 2.022$.

On the other hand, transient chaos and bursting oscillation, as two special dynamical phenomena, has been reported in some nonlinear systems [35]. Interestingly, the system exhibits complex transient chaos and periodic bursting behaviors when choosing appropriate parameters and initial conditions. When taking as $a = 10, b = 20, c = 1, r = 1$ and the initial conditions $(0.2, 0.2, 0.2, 0.2)$, the time series and the corresponding phase portraits are plotted in Figs 8a–8d,

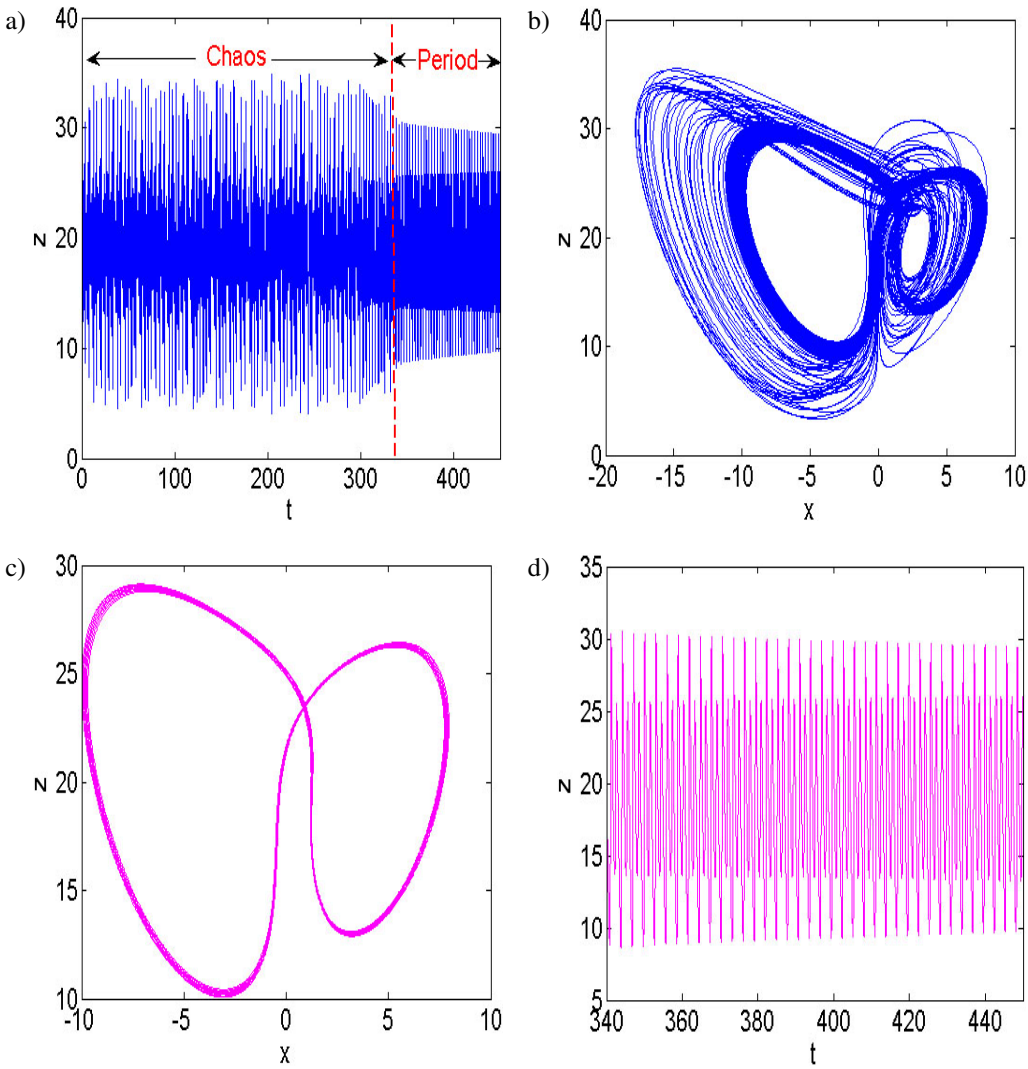

Figure 8: Transient chaos behavior of the system (1): a) the time series of the state variable z, b) the corresponding phase portrait in the (x, z) plane, c) the phase portrait in the (x, z) plane in the region of $[340, 450]$s, d) the time series of the state z in the region of $[340, 450]$s.

respectively. From Fig. 8a, it can be seen that the system has a transition from transient chaos to steady period with the time evolution. What's more, when selecting $a = 1.5$, $b = 20$, $c = 1$, $r = 1$ and the initial conditions (0.2, 0.2, 0.2, 0.2), the system exhibits the distinctive phenomenon of periodic bursting as shown in Fig. 9. From the above analysis, we can conclude that the system indeed displays extremely complicated dynamics.

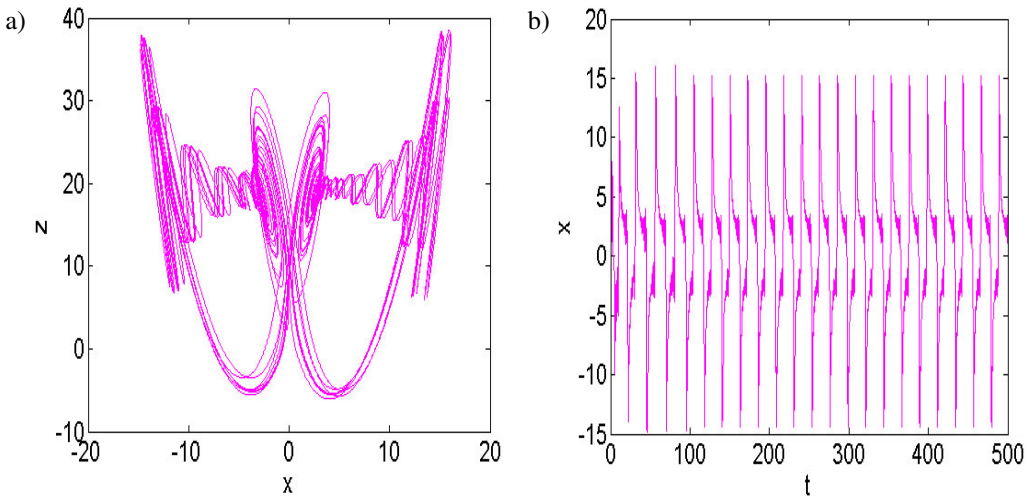

Figure 9: Periodic bursting oscillation of the system (1): a) the phase portrait in the (x, z) plane, b) the time series of the state x.

4. Chaos synchronization of the new 4-D chaotic system

As a control application, this section details the control design of achieving global chaos synchronization of the new 4-D chaotic system with itself via Integral Sliding Mode Control (ISMC) [36].

As the drive system of the synchronization process, we focus on the nonlinear plant

$$\begin{cases} \dot{x}_1 = a(y_1 - x_1) + w_1, \\ \dot{y}_1 = x_1(b - z_1), \\ \dot{z}_1 = x_1 y_1 - c z_1, \\ \dot{w}_1 = r - a y_1 - w_1, \end{cases} \tag{15}$$

where $X_1 = [x_1, y_1, z_1, w_1]^T$ is the state vector and a, b, c, r are constant parameters.

As the drive system of the synchronization process, we focus on the nonlinear plant

$$\begin{cases} \dot{x}_2 &= a(y_2 - x_2) + w_2 + \varphi_x\,, \\ \dot{y}_2 &= x_2(b - z_2) + \varphi_y\,, \\ \dot{z}_2 &= x_2 y_2 - c z_2 + \varphi_z\,, \\ \dot{w}_2 &= r - a y_2 - w_2 + \varphi_w\,, \end{cases} \tag{16}$$

where $X_2 = [x_2, y_2, z_2, w_2]^T$ is the state vector and $\varphi_x, \varphi_y, \varphi_z, \varphi_w$ serve as the sliding controls.

We shall next define the synchronization error between the drive system (15) and the response system (16) in the following manner:

$$\begin{cases} e_x &= x_2 - x_1\,, \\ e_y &= y_2 - y_1\,, \\ e_z &= z_2 - z_1\,, \\ e_w &= w_2 - w_1\,. \end{cases} \tag{17}$$

It follows that we can derive the synchronization error between the two 4-D nonlinear plants (15) and (16) as follows:

$$\begin{cases} \dot{e}_x &= a(e_y - e_x) + e_w + \varphi_x\,, \\ \dot{e}_y &= b e_x - x_2 z_2 + x_1 z_1 + \varphi_y\,, \\ \dot{e}_z &= -c e_z + x_2 y_2 - x_1 y_1 + \varphi_z\,, \\ \dot{e}_w &= -a e_y - e_w + \varphi_w\,. \end{cases} \tag{18}$$

The integral sliding surface associated with each error variable can be classified by the following equations.

$$\begin{cases} s_x &= e_x + \lambda_x \displaystyle\int_0^t e_x(\tau)\,\mathrm{d}\tau, \\ s_y &= e_y + \lambda_y \displaystyle\int_0^t e_y(\tau)\,\mathrm{d}\tau, \\ s_z &= e_z + \lambda_z \displaystyle\int_0^t e_z(\tau)\,\mathrm{d}\tau, \\ s_w &= e_w + \lambda_w \displaystyle\int_0^t e_w(\tau)\,\mathrm{d}\tau. \end{cases} \tag{19}$$

Using (19), we derive the differential equations of the integral sliding surfaces as follows:

$$\begin{cases} \dot{s}_x &= \dot{e}_x + \lambda_x e_x, \\ \dot{s}_y &= \dot{e}_y + \lambda_y e_y, \\ \dot{s}_z &= \dot{e}_z + \lambda_z e_z, \\ \dot{s}_w &= \dot{e}_w + \lambda_w e_w. \end{cases} \tag{20}$$

We assume that $\lambda_x, \lambda_y, \lambda_z, \lambda_z$ are positive conditions. Thus, the Hurwitz condition is satisfied.

Using integral sliding mode control [36], we take the feedback control law as

$$\begin{cases} \varphi_x &= -a(e_y - e_x) - e_w - \lambda_x e_x - \eta_x \mathrm{sgn}(s_x) - k_x s_x, \\ \varphi_y &= -be_x + x_2 z_2 - x_1 z_1 - \lambda_y e_y - \eta_y \mathrm{sgn}(s_y) - k_y s_y, \\ \varphi_z &= ce_z - x_2 y_2 + x_1 y_1 - \lambda_z e_z - \eta_z \mathrm{sgn}(s_z) - k_z s_z, \\ \varphi_w &= ae_y + e_w - \lambda_w e_w - \eta_w \mathrm{sgn}(s_w) - k_w s_w. \end{cases} \tag{21}$$

Substitution of the control law (21) into (18) yields the closed-loop system

$$\begin{cases} \dot{e}_x &= -\lambda_x e_x - \eta_x \mathrm{sgn}(s_x) - k_x s_x, \\ \dot{e}_y &= -\lambda_y e_y - \eta_y \mathrm{sgn}(s_y) - k_y s_y, \\ \dot{e}_z &= -\lambda_z e_z - \eta_z \mathrm{sgn}(s_z) - k_z s_z, \\ \dot{e}_w &= -\lambda_w e_w - \eta_w \mathrm{sgn}(s_w) - k_w s_w. \end{cases} \tag{22}$$

The main result of this section is proved next.

Theorem 1 *The new 4-D systems (15) and (16) are globally and asymptotically synchronized for all initial values by the integral SMC law (21) where* λ_x, λ_y, λ_z, λ_w, k_x, k_y, k_z, k_w, η_x, η_y, η_z, *and* η_w *are taken as positive constants.*

Proof. We consider the Lyapunov function defined by means of the following formula

$$V(s_x, s_y, s_z, s_w) = \frac{1}{2}\left(s_x^2 + s_y^2 + s_z^2\right). \tag{23}$$

It is obvious that V is a quadratic and positive definite function defined on $\mathbf{R}^4$.

The time-derivative of V along the error trajectories is calculated using (22) and (20) as follows:

$$\dot{V} = -\eta_x|s_x| - \eta_y|s_y| - \eta_z|s_z| - \eta_w|s_w| - k_x s_x^2 - k_y s_y^2 - k_z s_z^2 - k_w s_w^2 . \quad (24)$$

Thus, $\dot{V}$ is a negative definite function defined on $\mathbf{R}^4$.

Therefore, the proof is complete by Lyapunov stability theory [37]. □

For simulations, we take $k_x = k_y = k_z = k_w = 10$. We also take $\eta_x = \eta_y = \eta_z = \eta_w = 0.1$.

Furthermore, we take $\lambda_x = \lambda_y = \lambda_z = \lambda_w = 20$.

The initial state of the drive system (15) is taken as $x_1(0) = 5.4$, $y_1(0) = 3.1$, $z_1(0) = 1.8$ and $w_1(0) = 12.9$.

The initial state of the response system (15) is taken as $x_2(0) = 1.2$, $y_2(0) = 9.5$, $z_2(0) = 4.7$ and $w_2(0) = 0.4$.

Figures 10–13 depict the complete synchronization between the states of the 4-D systems (15) and (16), while Fig. 14 shows the time-plot of the synchronization error between the 4-D systems (15) and (16).

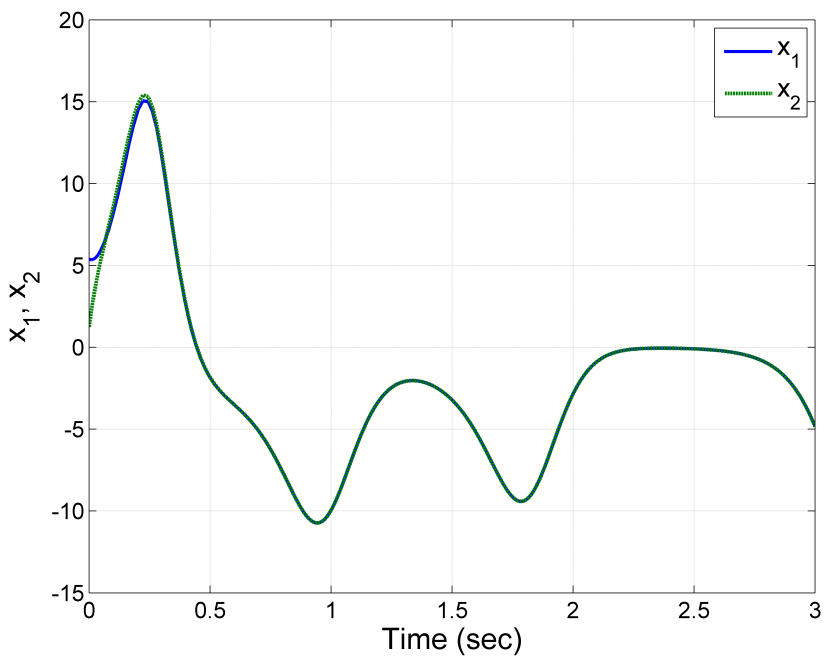

Figure 10: MATLAB plot showing the synchronization between the states x_1 and x_2 of the 4-D systems (15) and (16) for $X_1(0)$=(5.4, 3.1, 1.8, 12.9) and $X_2(0)$=(1.2, 9.5, 4.7, 0.4).

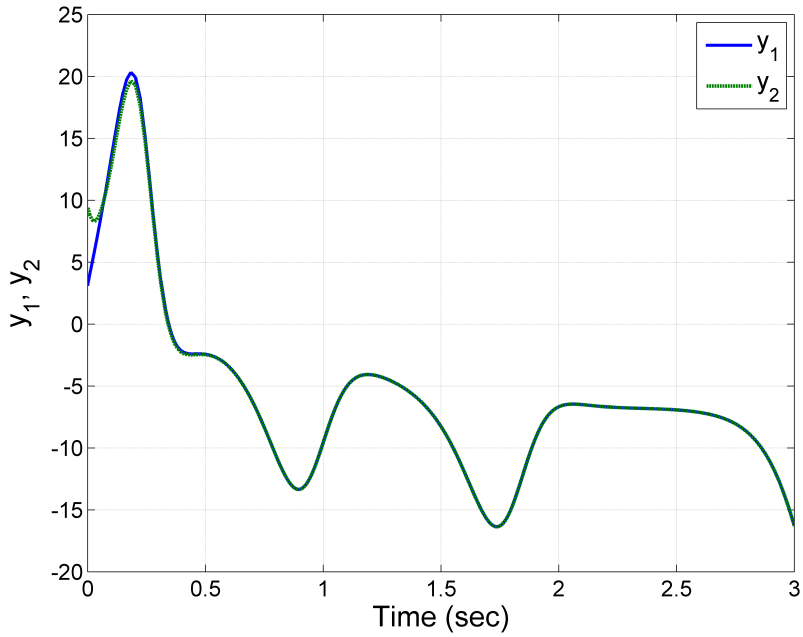

Figure 11: MATLAB plot showing the synchronization between the states y_1 and y_2 of the 4-D systems (15) and (16) for $X_1(0)$=(5.4, 3.1, 1.8, 12.9) and $X_2(0)$=(1.2, 9.5, 4.7, 0.4).

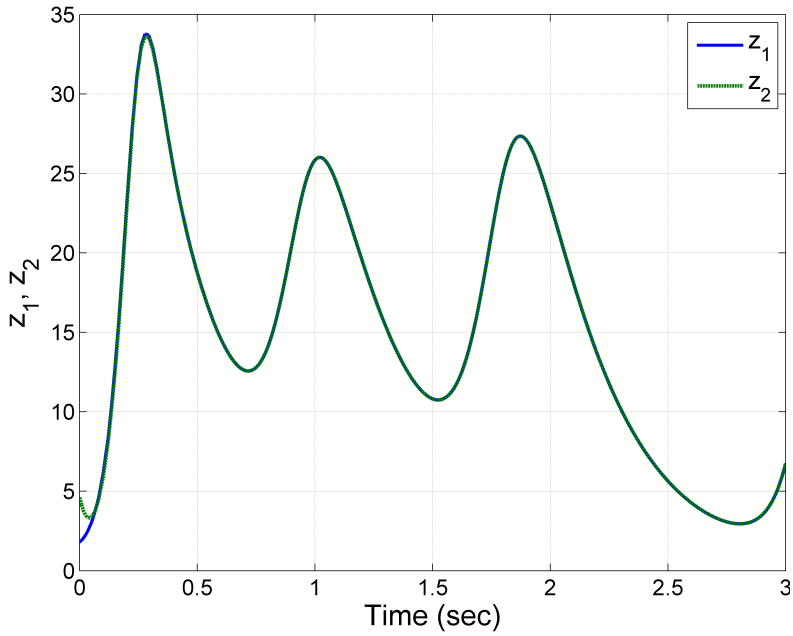

Figure 12: MATLAB plot showing the synchronization between the states z_1 and z_2 of the 4-D systems (15) and (16) for $X_1(0)$=(5.4, 3.1, 1.8, 12.9) and $X_2(0)$=(1.2, 9.5, 4.7, 0.4).

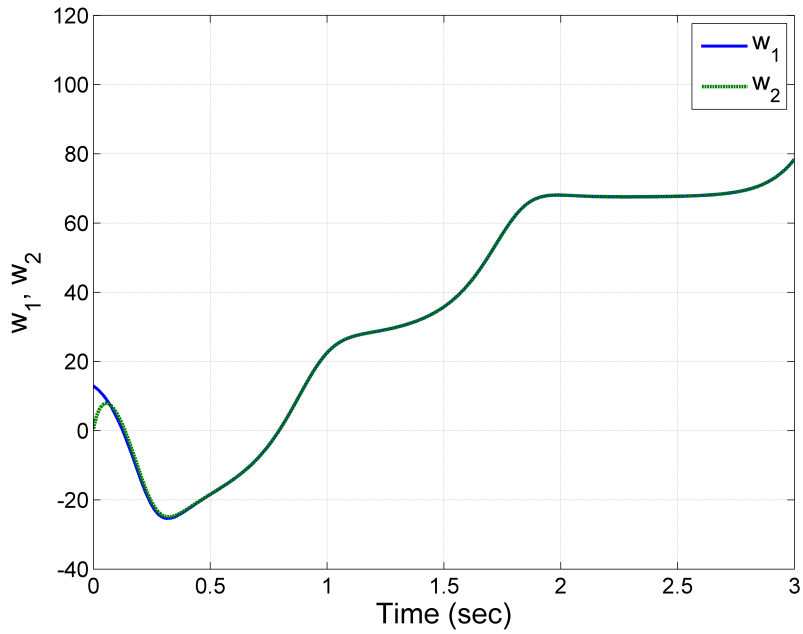

Figure 13: MATLAB plot showing the synchronization between the states w_1 and w_2 of the 4-D systems (15) and (16) for $X_1(0)$=(5.4, 3.1, 1.8, 12.9) and $X_2(0)$=(1.2, 9.5, 4.7, 0.4).

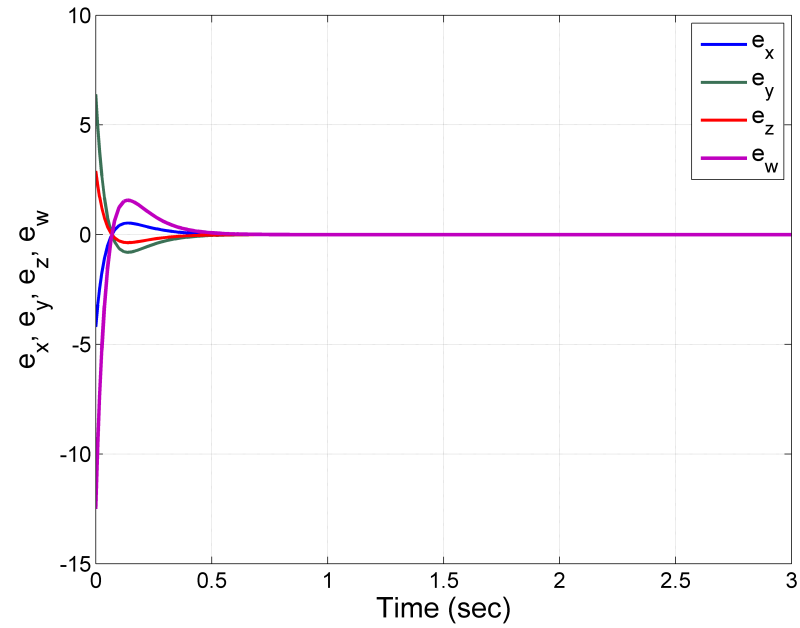

Figure 14: MATLAB plot showing the time-history of the synchronization error (e_x, e_y, e_z, e_w) between the 4-D systems (15) and (16) for $X_1(0)$=(5.4, 3.1, 1.8, 12.9) and $X_2(0)$=(1.2, 9.5, 4.7, 0.4).

5. Circuit simulation of the new 4-D chaotic system

The implementation of electronic circuits using chaotic signals has been investigated in various engineering applications such as secure communication system [38], robotics [39] and high frequency generator [40]. In this work, the four state variables of system (1) x, y, z, w are rescaled. As a result, we transform system (1) into system (25):

$$\begin{cases} \dot{x} = a(y-x)+2w, \\ \dot{y} = x(b-2z), \\ \dot{z} = 2xy-cz, \\ \dot{w} = \dfrac{r}{4}-\dfrac{ay}{2}-w. \end{cases} \tag{25}$$

In (25), $X=\dfrac{1}{2}x$, $Y=\dfrac{1}{2}y$, $Z=\dfrac{1}{2}z$, and $W=\dfrac{1}{4}w$. In this case, we take $r=0$ for chaotic system with line equilibrium. By applying Kirchhoff's circuit laws into the circuit of Fig. 15, we get its circuital equations:

$$\begin{cases} \dot{X} = \dfrac{1}{C_1R_1}Y-\dfrac{1}{C_1R_2}X+\dfrac{1}{C_1R_3}W, \\ \dot{Y} = \dfrac{1}{C_2R_4}X-\dfrac{1}{10C_2R_5}XZ, \\ \dot{Z} = \dfrac{1}{10C_3R_6}XY-\dfrac{1}{C_3R_7}Z, \\ \dot{W} = -\dfrac{1}{C_4R_8}Y-\dfrac{1}{C_4R_9}W. \end{cases} \tag{26}$$

We note that X, Y, Z and W correspond to the voltages on the integrators U1A, U2A, U3A and U4A, respectively. The values of components in the circuit are selected as: $R_1 = R_2 = 40$ kΩ, $R_3 = 200$ kΩ, $R_4 = R_5 = R_6 = 20$ kΩ, $R_7 = 133.33$ kΩ, $R_8 = 80$ kΩ, $R_9 = 400$ kΩ, $R_{10} = R_{11} = R_{12} = R_{13} = R_{14} = R_{15} = 100$ kΩ, $C_1 = C_2 = C_3 = C_4 = 1$ nF. MultiSIM outputs of the circuit are presented in Fig. 16. The MultiSIM simulation results (see Fig. 16) show a good match with the MATLAB simulation of the 4-D chaotic system in Section 2 (see Figs 1–4).

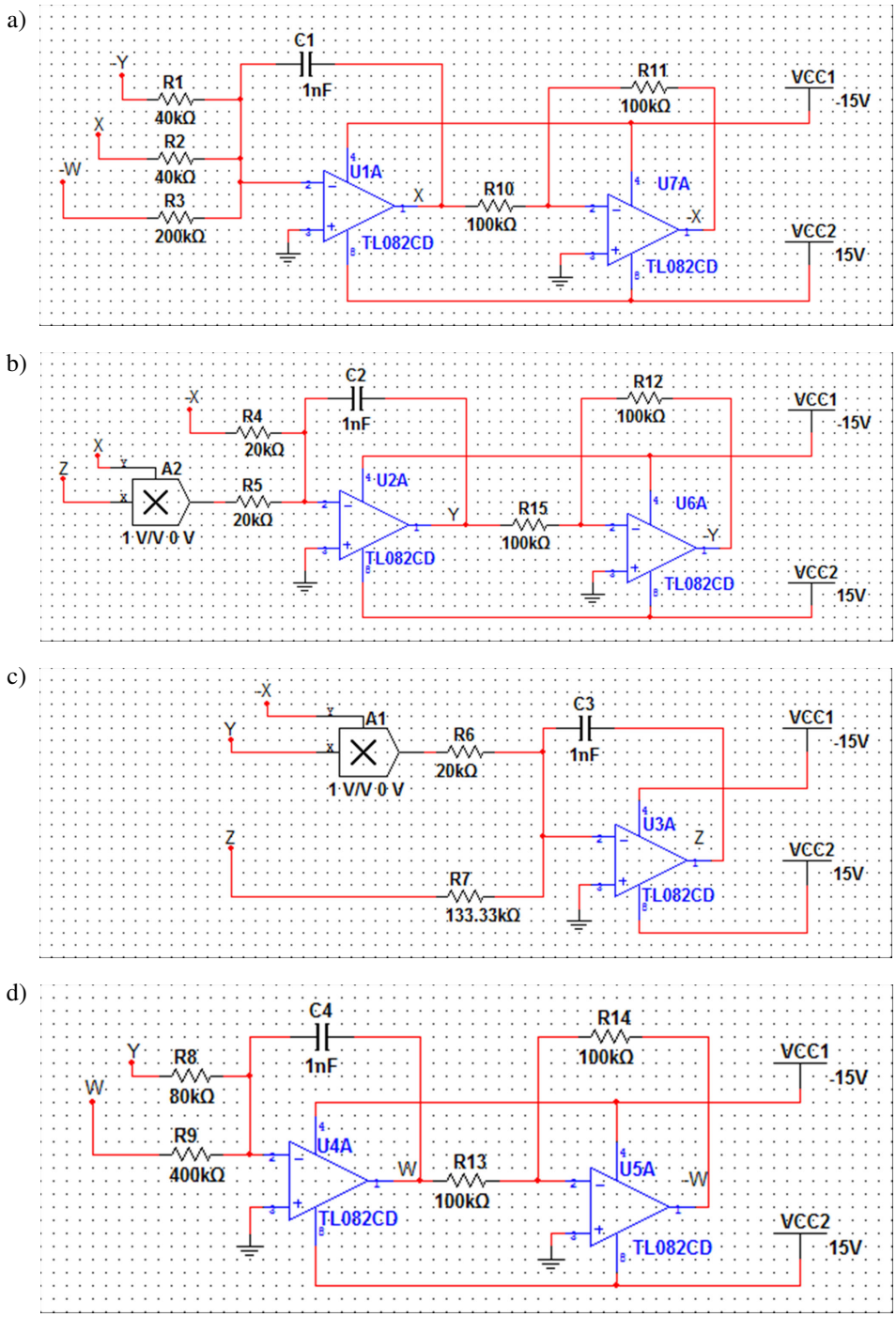

Figure 15: Circuit design of the new 4D chaotic system (1): a) X signal, b) Y signal, c) Z signal and d) W signal.

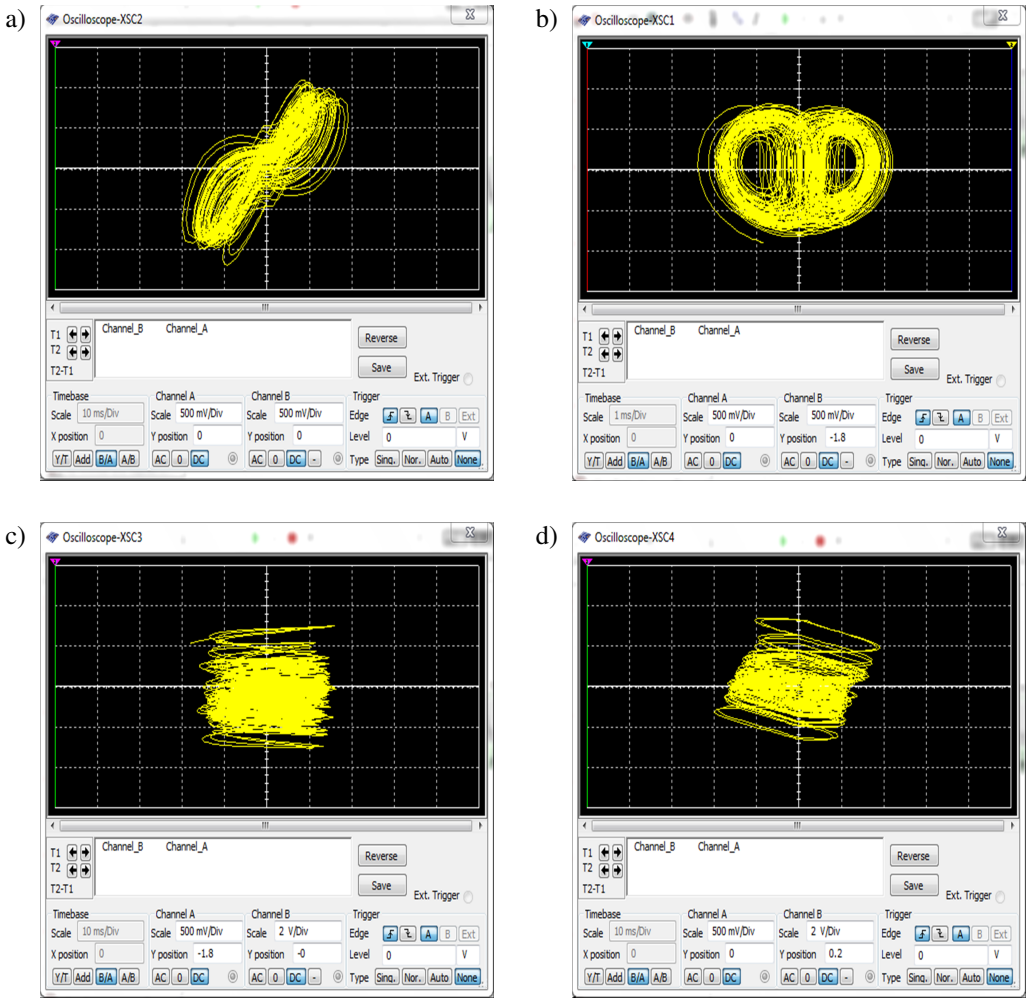

Figure 16: Chaotic attractors of system (1) using MultiSIM circuit simulation: a) $X-Y$ plane, b) $Y-Z$ plane, c) $Z-W$ plane and d) $X-W$ plane.

6. Conclusions

This work presented a new 4-D dynamical system exhibiting chaos. It was proved that the new nonlinear plant has an unstable rest point and a line of rest points. Thus, it is concluded that the new nonlinear plant exhibits hidden attractors. A detailed dynamic analysis of the new nonlinear plant using bifurcation diagrams was carried out. Synchronization result of the new nonlinear plant with itself was worked out using Integral Sliding Mode Control (ISMC). Finally, a circuit model using MultiSim of the new 4-D nonlinear plant with chaos was done for practical use.

References

[1] A.T. Azar, A. Radwan, and S. Vaidyanthan: *Mathematical Techniques of Fractional Order Systems*. Amsterdam, Elsevier, 2018.

[2] V.T. Pham, S. Vaidyanathan, C. Volos, and T. Kapitaniak: *Nonlinear Dynamical Systems with Self-Excited and Hidden Attractors*. Berlin, Springer, 2018.

[3] S. Vaidyanathan: Hyperchaos, qualitative analysis, control and synchronisation of a ten-term 4-D hyperchaotic system with an exponential nonlinearity and three quadratic nonlinearities. *International Journal of Modelling, Identification and Control*, **23**(4), (2015), 380–392.

[4] S. Vaidyanathan: Adaptive controller and synchronizer design for the Qi-Chen chaotic system. *Lecture Notes of the Institute for Computer Sciences, Social-Informatics and Telecommunications Engineering*, **85** (2012), 124–133.

[5] S. Vaidyanathan: Analysis, control, and synchronization of a 3-D novel jerk chaotic system with two quadratic nonlinearities. *Kyungpook Mathematical Journal*, **55**(3), (2015), 563–586.

[6] S. Pakiriswamy and S. Vaidyanathan: Generalized projective synchronization of three-scroll chaotic systems via active control. *Lecture Notes of the Institute for Computer Sciences, Social-Informatics and Telecommunications Engineering*, **85** (2012), 146–155.

[7] S. Vaidyanathan: Output regulation of the forced Van der Pol chaotic oscillator via adaptive control method. *International Journal of PharmTech Research*, **8**(6), (2015), 106–116.

[8] D.M. Wang, L.S. Wang, Y.Y. Guo, Y.C. Wang, and A.B. Wang: Key space enhancement of optical chaos secure communication: Chirped FBG feedback semiconductor laser. *Optics Express*, **27**(3), (2019), 3065–3073.

[9] Z.X. Liu, C. You, B. Wang, H. Xiong, and Y. Wu: Phase-mediated magnon chaos-order transition in cavity optomagnonics. *Optics Letters*, **44**(3), (2019), 507–510.

[10] S. Vaidyanathan: Adaptive control of the FitzHugh-Nagumo chaotic neuron model. *International Journal of PharmTech Research*, **8**(6), (2015), 117–127.

[11] S. Vaidyanathan: Chaos in neurons and synchronization of Birkhoff-Shaw strange chaotic attractors via adaptive control. *International Journal of PharmTech Research*, **8**(6), (2015), 1–11.

[12] S. Vaidyanathan: Adaptive chaotic synchronization of enzymes-substrates system with ferroelectric behaviour in brain waves. *International Journal of PharmTech Research*, **8**(5), (2015), 964–973.

[13] S. Dash, M.N. Das, and M. Das: Secured image transmission through region-based steganography using chaotic encryption. *Advances in Intelligent Systems Computing*, **711** (2019), 535–544.

[14] R. Banupriya, J. Deepa, and S. Suganthi: Video steganography using LSB algorithm for security application. *International Journal of Mechanical Engineering and Technology*, **10**(1), (2019), 203–211.

[15] X. Wang, H. Zhao, and M. Wang: A new image encryption algorithm with nonlinear-diffusion based on multiple coupled map lattices. *Optics and Laser Technology*, **115** (2019), 42–57.

[16] T. Sivakumar and P. Li: A secure image encryption method using scan pattern and random key stream derived from laser chaos. *Optics and Laser Technology*, **111** (2019), 196–204.

[17] S. Vaidyanathan: A novel chemical chaotic reactor system and its adaptive control. *International Journal of ChemTech Research*, **8**(7), (2015), 146–158.

[18] S. Vaidyanathan: A novel chemical chaotic reactor system and its output regulation via integral sliding mode control. *International Journal of ChemTech Research*, **8**(11), (2015), 669–683.

[19] S. Vaidyanathan: Global chaos synchronization of chemical chaotic reactors via novel sliding mode control method. *International Journal of ChemTech Research*, **8**(7), (2015), 209–221.

[20] S. Vaidyanathan: Lotka-Volterra population biology models with negative feedback and their ecological monitoring. *International Journal of PharmTech Research*, **8**(5), (2015), 974–981.

[21] O.I. Tacha, C.K. Volos, I.M. Kyprianidis, I.N. Stouboulos, S. Vaidyanathan, and V.T. Pham: Analysis, adaptive control and circuit simulation of a novel nonlinear finance system. *Applied Mathematics and Computation*, **276** (2016), 200–217.

[22] F. Liu: Unconventional direct acquisition method for chaotic DSSS signals. *AEU – International Journal of Electronics and Communications*, **99** (2019), 293–298.

[23] X.Y. Wang and Z.M. Li: A color image encryption algorithm based on Hopfield chaotic neural network. *Optics and Lasers in Engineering*, **115** (2019), 107–118.

[24] Z. Hua, Y. Zhou, and H. Huang: Cosine-transform-based chaotic system for image encryption. *Information Sciences*, **480** (2019), 403–419.

[25] P.S. Gohari, H. Mohammadi, and S. Taghvaei: Using chaotic maps for 3D boundary surveillance by quadrotor robot. *Applied Soft Computing*, **76** (2019), 68–77.

[26] Y. Naseer, D. Shah, and T. Shah: A novel approach to improve multimedia security utilizing 3D mixed chaotic map. *Microprocessors and Microsystems*, **65** (2019), 1–6.

[27] B. Karakaya, A. Gulten, and M. Frasca: A true random bit generator based on a memristive chaotic circuit: Analysis, design and FPGA implementation. *Chaos, Solitons and Fractals*, **119** (2019), 143–149.

[28] H. Wang and G. Dong: New dynamics coined in a 4-D quadratic autonomous hyper-chaotic system. *Applied Mathematics and Computation*, **346** (2019), 272–286.

[29] S. Vaidyanathan: Analysis and synchronization of the hyperchaotic Yujun systems via sliding mode control. *Advances in Intelligent Systems and Computing*, **176** (2012), 329–337.

[30] S. Vaidyanathan, C. Volos, and V.T. Pham: Global chaos control of a novel nine-term chaotic system via sliding mode control. *Studies in Computational Intelligence*, **576** (2015), 571–590.

[31] S. Zhang, Y.C. Zeng, and Z.J. Li: Chaos in a novel fractional order system without a linear term. *International Journal of Non-Linear Mechanics*, **106** (2018), 1–12.

[32] S. Zhang, Y.C. Zeng, Z.J. Li, M.J. Wang, X. Zhang, and D. Chang: A novel simple no-equilibrium chaotic system with complex hidden dynamics. *International Journal of Dynamics and Control*, **23** (2018), 1–12.

[33] S. Zhang, Y.C. Zeng, and Z.J. Li: One to four-wing chaotic attractors coined from a novel 3D fractional-order chaotic system with complex dynamic. *Chinese Journal of Physics*, **56** (2018), 793–806.

[34] L. Wang, S. Zhang, Y.C. Zeng, and Z.J. Li: Generating hidden extreme multistability in memristive chaotic oscillator via micro-perturbation. *Electron letters*, **52** (2018), 1008–1010.

[35] S. Zhang and Y.C. Zeng: A simple jerk-like system without equilibrium: Asymmetric coexisting hidden attractors, bursting oscillation and double full Feigenbaum remerging trees. *Chaos, Solitons and Fractals*, **120** (2019), 25–40.

[36] S. Vaidyanthan and C.H. Lien: *Applications of Sliding Mode Control in Science and Engineering*. Berlin, Springer, 2017.

[37] W.M. Haddad and V.S. Chellaboina: *Nonlinear Dynamical Systems and Control: A Lyapunov-Based Approach*. Princeton University Press, Princeton, 2008.

[38] A. Sambas, S. Vaidyanathan, M. Mamat, W.S.M. Sanjaya, and D.S. Rahayu: A 3-D novel jerk chaotic system and its application in secure communication system and mobile robot navigation. *Studies in Computational Intelligence*, **636** (2016), 283–310.

[39] S. Vaidyanathan, A. Sambas, M. Mamat, and W.S.M. Sanjaya: A new three-dimensional chaotic system with a hidden attractor, circuit design and application in wireless mobile robot. *Archives of Control Sciences*, **27** (2017), 541–554.

[40] A.S. Elwakil and M.P. Kennedy: High frequency Wien-type chaotic oscillator. *Electronics Letters*, **34** (1998), 1161–1162.